The contribution of femtosecond laser filaments to positive and negative breakdown discharge in a long air gap

Article in Physics of Plasma · April 2023

DOI: 10.1063/5.0138646

11 authors, including:

Zhehao Pei
Xi'an Jiaotong University

Xing Fan
Xi'an Jiaotong University

Jianwei Gu
China Electric Power Research Institute

Shengxin Huang
Hefei University of Technology

Physics of Plasmas

The contribution of femtosecond laser filaments to positive and negative breakdown discharge in a long air gap

Cite as: Phys. Plasmas **30**, 043511 (2023); https://doi.org/10.1063/5.0138646
Submitted: 13 December 2022 • Accepted: 29 March 2023 • Published Online: 14 April 2023

Zhehao Pei, Weijiang Chen, Xing Fan, et al.

Physics of Plasmas ARTICLE scitation.org/journal/php

The contribution of femtosecond laser filaments to positive and negative breakdown discharge in a long air gap

Cite as: Phys. Plasmas **30**, 043511 (2023); doi: 10.1063/5.0138646
Submitted: 13 December 2022 · Accepted: 29 March 2023 ·
Published Online: 14 April 2023

View Online Export Citation CrossMark

Zhehao Pei,[1] Weijiang Chen,[2,a)] Xing Fan,[1] Jianwei Gu,[3] Shengxin Huang,[4] Xiaosong Liu,[1] Zhong Fu,[5] Bin Du,[4] Tiejun Wang,[6] Rui Zhang,[1] and Qiaogen Zhang[1]

AFFILIATIONS

[1]State Key Laboratory of Electrical Insulation and Power Equipment, Xi'an Jiaotong University, Xi'an 710049, China
[2]State Grid Corporation of China, Beijing 100031, China
[3]High Voltage Department, China Electric Power Research Institute, Beijing 100032, China
[4]School of Electrical Engineering and Automation, Hefei University of Technology, Hefei 230009, China
[5]Electric Power Research Institute, State Grid Anhui Electric Power Company, Hefei 230601, China
[6]State Key Laboratory of High Field Laser Physics, Shanghai Institute of Optics and Fine Mechanics and CAS Center for Excellence in Ultra-intense Laser Science, Chinese Academy of Sciences, Shanghai 201899, China

[a)]Author to whom correspondence should be addressed: wj_chen@yeah.net

ABSTRACT

Discharges of different polarities develop in different modes, resulting in different guiding effects by femtosecond laser filaments. Knowledge of the contribution of laser filaments to positive and negative discharges is the basis of the laser-guided long-air-gap discharge technique. This study presents a direct comparison of the inception, propagation, and breakdown characteristics of discharges of both polarities. Long-air-gap discharge experiments under the switching impulses of both polarities are carried out under the same experimental conditions. Discharge modes and phases are also considered. The statistical results show that positive discharge inception voltages are transformed from a Weibull distribution into an exponential distribution under the influence of laser filaments, but there is little effect on the negative discharge inception voltage. The guidance probability of a positive discharge reaches 15% at most during the dark period stage, leading to little effect on the breakdown discharge probability. However, for negative discharges, the guidance probability can exceed 95%. An investigation of the filament contributions to both polarity discharges shows that the different migration directions of photoelectrons lead to a difference in the effects of laser filaments on inception voltages, and the difference in the connection of the two discharge passages leads to a difference in the guidance probability. Through the results of a simulation model, it is speculated that the connection condition for positive discharges is that the positive leader overlaps with the laser filaments, and, for negative discharges, the rod electrode is connected to the laser filaments through bi-directional discharge propagation.

I. INTRODUCTION

Cloud-ground lightning strikes are a huge threat to important facilities such as oil fields, refineries, airports, launchpads, power supply systems, and distribution systems.[1] Lightning discharge is highly random and dispersed, with temporal and spatial characteristics that cannot be accurately predicted or controlled, causing huge difficulties in lightning protection. Mature methods, such as lightning rods or lightning wires, are not robust enough for high lightning protection demands.[2] To further improve lightning protection systems, active lightning protection methods[3] that can improve the success rate and reliability of lightning attraction by guiding the lightning discharge path have been proposed. Both conductors[4] and plasma passages[5] work for this purpose. Plasma passages, which can be generated by ultra-short-pulse lasers (with laser pulse widths $< 10^{-12}$ s)[6–8] due to their long propagation distances and high power densities, can affect the discharge process in the large-scale atmosphere.[9–12] Ultra-short-pulse laser guiding discharges are considered to be one of the most promising frontier technologies in the field of active lightning protection.

The physical process of a lightning discharge includes descending and ascending leaders. About 90% of all descending leader discharges are negative and roughly as many ascending discharges are positive.[1] Each polarity discharge develops through different mechanisms.[13–15] The technical route for guiding a lightning discharge can be divided into two types: the guidance of descending negative discharge and of ascending positive discharge.

Studies on laser filaments applied to both polarity discharges have been conducted. The first investigations on the influence of lasers on the free-stable propagation of leader discharges were conducted using laser-induced discharge experiments in 3–7 m rod-plate gap discharge circuits.[16] The distributions of positive-polarity voltages of the streamer initiation during different moments of the laser triggering process were obtained. Four impact regimes were proposed, depending on the laser shot timing. When the electric field was too weak, a corona could be triggered after a certain delay, and the leader discharge could not form. When the electric field was slightly stronger but still before the natural inception of the first corona, a corona could be instantaneously triggered by a laser shot. When the laser pulse was triggered during the dark period, intermittent low-probability induction could be achieved. When the laser pulse was sent after a natural leader propagation phase, it had no effect. The abilities of laser filaments to affect positive corona inception and leader inception at different phases of natural positive discharge were clarified, providing important experimental data on laser-induced positive-polarity discharges.

Negative discharges develop in a different mode. Previous studies have shown that a negative discharge can develop along the space stem generated by laser filaments.[17] The sphere-plane gap was seen to expand from 2.3 to 4.5 m and to provoke a space stem observed through a fast-frame camera. The research team of Teramobile compared two polarity discharge characteristics under the influence of laser filaments with fixed conditions.[18] A 4 μs wavefront lightning pulse was applied to a 2.5 m sphere-plane gap. The decreased breakdown field percentage of negative discharges was shown to be much larger than that of positive discharges. Furthermore, an experimental campaign carried out on Säntis Mountain in Northeastern Switzerland observed only negatively charged ascending discharges.[19] It is easier to bridge the gap between filaments and a negative discharge than a positive discharge connected with a lightning rod. Based on a large amount of experimental experience,[20–31] it has become clear that the contributions of laser filaments to positive and negative discharges are different. However, the reason for the difference in the induction results of positive and negative discharges in long air gaps has not yet been determined. It would thus be meaningful to accumulate more comparison statistics regarding the two polarity discharges under the same experimental conditions to clarify this mechanism.

In this study, to comprehensively determine the contribution of laser filaments to both positive and negative discharges, long-air-gap discharge experiments under switching impulses of both polarities are performed under the same experimental conditions. Discharge modes and phases are also considered. The time intervals for applying a femtosecond laser are based on the natural discharge phases. The inception and propagation characteristics of natural discharges with laser-influenced discharges are compared. The discharge characteristics during similar discharge periods under positive and negative-polarity voltages are also compared. Statistical data are used to analyze the discharge characteristics to shed light on the underlying mechanisms.

II. EXPERIMENTAL SETUP

All experiments were conducted indoors at the Ultra High Voltage Test Hall of the Anhui Electric Power Research Institute. A schematic of the experimental setup is provided in Fig. 1. For the effective generation of leader initiation and development, a 2 m rod-plate gap was adopted and a 4.8 MV Marx generator was employed as a high-voltage source for generating standard voltage impulses (250/2500 μs) to the rod-plate gap. The rod electrode was 4 m above the ground, and the 4×4 m^2 plate electrode was 2 m above the ground. Through a 30 mm radius circular hole, the laser beam propagated from the grounded plate electrode toward the rod electrode, forming an angle α with the central axis. The laser system delivered pulses of 100 mJ with pulse durations down to 35 fs. The central wavelength was 800 nm and the repetition rate was 10 Hz. For the experiments, a 70 mJ/56 fs laser pulse was applied. The energy involved was tested by an energy meter and the pulse duration by an autocorrelator. After the laser passed through a 5 m focal lens, a 1.5 m laser filament was formed in the gap, which stayed 1 cm away from the rod electrode. At 800 nm, the photon energy of the laser was around 1.5 eV, and the effective nonlinear order of the multiphoton ionization of air was around 8. The electron energy is the sum of the potential energy, which is equal to the atom's ionization potential, and the kinetic energy absorbed from the excess energy of the laser field, also called the above-threshold ionization (ATI).[32] The mean average ATI energy can be expressed as $U_{ATI} = \frac{U_p}{K'+1}$, where U_p is the pondermotive energy, and K' is an effective number of photons. In this case, U_{ATI} could be estimated to be around 0.5 eV. The electron energy distribution can be found in Sergey's work.[33] Through multiphoton ionization, free electrons can be provided with low kinetic energy in the focal area at one atmospheric pressure. Due to the mean free time of a released free electron, which was calculated as 300–800 fs, being longer than the pulse duration, no inverse Bremsstrahlung or cascade ionization was expected to occur. The peak electron density of the filament was obtained through experiments to be above 10^{15} cm^{-3}. This is based on the charge collection method, which will be discussed in future work. Defining O as the coordinate origin, the closest position to the rod electrode, and the laser propagation direction as the positive direction of the x axis, d_{fr} represents the geometric focal point displacement from position O. For example, $d_{fr} = 0$ in Fig. 1. This parameter was used to characterize the relative positions of the laser plasma and rod electrode.

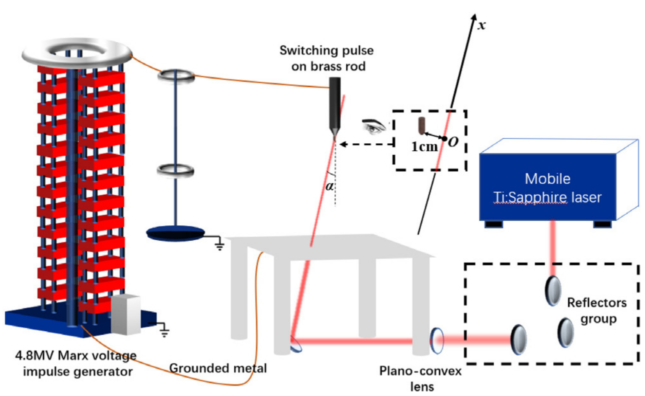

FIG. 1. Experimental setup.

The time intervals between adjacent laser beams reached up to 100 ms, which is much larger than the dissipation times of the filament plasma and discharge passage. Thus, this influence was regarded as a contribution from the single laser filament. The time delay between the laser shot and the voltage impulse was synchronized using a synchronization system formed by the DG535, a 10 kV voltage pulse trigger device, and photoelectric conversion devices. The jitter of the delay was controlled to within 20 μs, which mainly came from the voltage generator. The discharge current was recorded by a current measurement device made of a coaxial resistance shunt and a digital signal optical fiber transmission system. The coaxial resistance shunt consisted of ten non-inductance resistors in parallel. Its equivalent resistance was 5 Ω, its frequency bandwidth was DC-18.3 MHz, and its measurement range was -40 to 40 A. A high-speed camera with a Nikon lens (8–48 mm, *f*/1.0) was placed at a distance of 8 m from the discharge gap, with a maximum frame rate of 2 000 000 frames/s. In the experiment, 300 000 frames per second with a frame size of 256×128 pixels were used to capture the images of the discharge processes. The environmental conditions were as follows: atmospheric pressure ~ 1 atm, temperature 13–18 °C, and relative humidity 61%–74%, corresponding to an absolute humidity of 6.91–11.36 g/cm^{-3}.

III. DISCHARGE CHARACTERISTICS

A. Inception voltage

The discharge process in a long air gap can be divided into two phases: inception and development. For positive-polarity discharge, the first streamer occurs during the inception phase and the development phase depends on continuous stable leader inception and leader propagation. For negative-polarity discharge, the first streamer occurs during the inception phase, which is common with positive discharge, while the development phase depends on negative leader propagation as well as the connection between the space stem and negative discharge.

Among the aforementioned discharge modes, the first streamer discharge is only affected by the applied electric field without any influence from space charge, which can reflect the electric field and has an impact on the subsequent discharge processes. In this study, the inception voltage was used to characterize the first streamer process.

1. Positive-polarity inception voltage

Thirty tests were performed on the rod-plate discharge gap under a positive-polarity voltage impulse to obtain the inception voltage. The moment the current signal rose steeply from 0 was regarded as the inception moment, and the voltage amplitude at the inception moment was taken as the inception voltage. To eliminate the effect of residual charge on the next discharge event, the test interval was set to be greater than 3 min. The peak value of the applied voltage was selected to be 50% of the discharge voltage, ~ 821 kV. The measured inception voltages and statistical analysis were collected and analyzed [Figs. 2(a)–2(f)]. Histograms of the probability density distribution showed that the positive streamer inception voltage covered a wide span from 158 to 289 kV. The large dispersion reflected the strong stochastic nature of the first streamer inception.

Five probability models have been used previously to describe the statistical behavior of a positive streamer inception voltage, including the Weibull distribution [$X \sim \Omega(k, \eta)$], normal distribution [$X \sim N(\mu, \sigma 2)$], normal logarithmic distribution [$\ln X \sim N(\mu, \sigma 2)$], exponential distribution [$X \sim E(1/\lambda)$], and Gamma distribution [$X \sim \Gamma(\alpha, \beta)$]. The aforementioned probability density functions and descriptions of their parameters can be found in previous studies.[34] The distribution parameter values of each probability model were estimated based on the first streamer inception voltage measurements [Fig. 2(a)]. The probabilities of the four distributions were derived from data curves and found to approximate the statistical patterns of the first streamer inception voltages, except in the case of the exponential distribution. To sufficiently determine the statistical distribution of the streamer inception voltages, Q–Q plots were created to further determine whether the measurement data obeyed the four probability distributions [Figs. 2(b)–2(f)]. The statistical parameters and Pearson correlation coefficients (*corr*P) are shown in each figure. The *corr*P of the Weibull distribution was 0.9915 and closest to 1 among the five distributions. The positive streamer inception voltage was, thus, more likely to fit the Weibull distribution.

The femtosecond laser propagated into the discharge gap before the streamer inception moment, with the time delay of the laser and voltage signals set from 0 to 10 μs. The peak value of the applied voltage was set to 50% of the discharge voltage, ~ 821 kV, as in the non-laser experiments. Thirty sets of discharge experiments were carried out, and the measured inception voltages were statistically analyzed (Fig. 3). The resulting histograms showed that the positive streamer inception voltages with a laser filament applied ranged from 76 to 91 kV. Compared to the non-laser cases, on the one hand, the average value decreased from 230.4 to 80.2 kV and the dispersion significantly decreased. On the other hand, the range decreased from 130.7 to 13.9 kV. Probability density curves were fitted, and the *corr*P parameters of each probability model were calculated. The *corr*P of the exponential distribution was 0.9647 and the closest to 1. The presence of a femtosecond laser filament had a great impact on the distribution pattern of the positive streamer inception voltages. With a laser filament generated from 0 to 10 μs, the positive streamer inception voltage was more likely to fit the exponential distribution.

The first leader discharge occurred via the electric field but was also contributed to by the space charge left by the preceding discharge. This made it more susceptible to environmental factors affected by the applied electric field, such as air temperature and humidity, while the continuous stable leader inception was affected not only by the externally applied field. To minimize environmental influences, all experiments were carried out on the same afternoon. The leader inception was characterized by the leader inception voltage. Based on current and voltage measurements, the moment that the current signal rose steeply from 0 was noted, a continuously maintained current was regarded as the inception moment, and the voltage amplitude at the inception moment was taken as the leader inception voltage [Figs. 4(a)–4(b)]. Histograms of the probability density distribution showed that, in non-laser cases, the dispersion of the leader inception voltage was much larger than the streamer inception voltage, which ranged from 286 to 755 kV. The Weibull distribution was used to describe the measurement data, fitting parameters, and probability distribution functions.

The femtosecond laser propagated into the discharge gap before the streamer inception, with the time delay of the laser and voltage signals set from 0 to 10 μs. Histograms showed that the positive leader inception voltage with a laser filament applied ranged from 241 to 422 kV. Compared to non-laser cases, on the one hand, the average value decreased from 612 to 303 kV, and the dispersion significantly

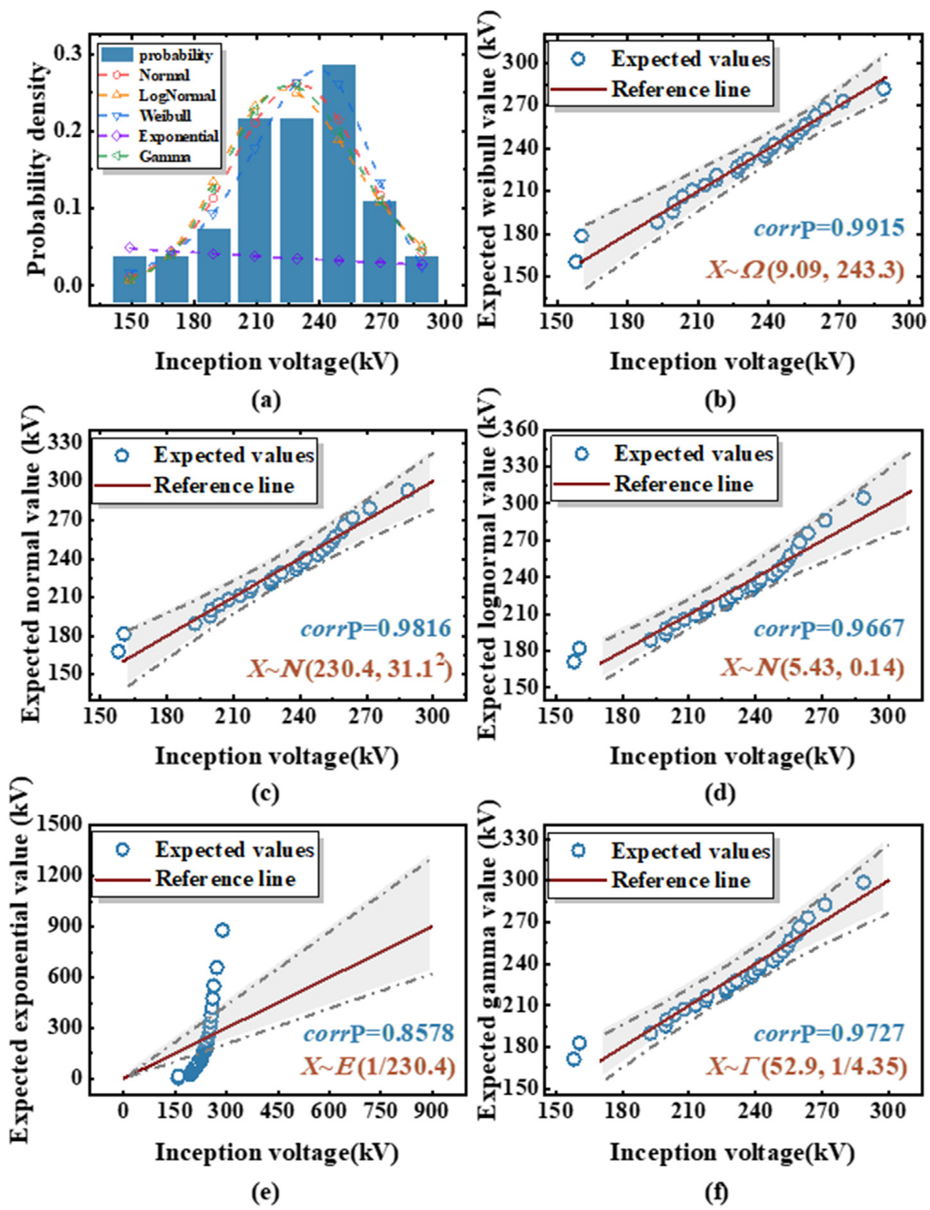

FIG. 2. Statistical analysis of the positive streamer inception voltage. (a) The probability density of the experimental data; (b) a Weibull distribution Q–Q plot; (c) a normal distribution Q–Q plot; (d) a lognormal distribution Q–Q plot; (e) an exponential distribution Q–Q plot; and (f) a Gamma distribution Q–Q plot. The dotted lines represent the 95% confidence bounds. The closer the correlation coefficient *corr*P was to 1, the more likely the inception voltage was to obey the probability distribution.

decreased. On the other hand, the range decreased from 469 to 181 kV, and the shape parameter of the Weibull distribution of the non-laser data decreased, as can be seen from the histograms. The distribution characteristics gradually degraded to an exponential distribution; that is, the effect of laser filaments on leader inception was much more significant than that of the space charges left behind by the first streamer or other pre-sequence discharges.

2. Negative-polarity inception voltage

Thirty tests were performed on the rod-plate discharge gap under negative-polarity voltage impulses to obtain the inception voltages. The moment the current signal rose steeply from 0 was regarded as the inception moment, and the voltage amplitude at the inception moment was regarded as the inception voltage. The test interval was set to greater than 3 min and the peak value of the applied voltage was set to 50% of the discharge voltage, $\sim$1815 kV (Fig. 5). Histograms of the probability density distribution showed that the negative streamer inception voltage covered a wide span, from -214 to 522 kV. The streamer inception voltage of the negative polarity was not much lower than that of the positive polarity because the amplitude of the negative impulse was 2.2 times greater than that of the positive polarity and the applied voltage wavefront was steeper.

The femtosecond laser propagated into the discharge gap before the streamer inception moment, with the time delay of the laser and voltage signals set from 0 to 10 μs. The peak value of the applied

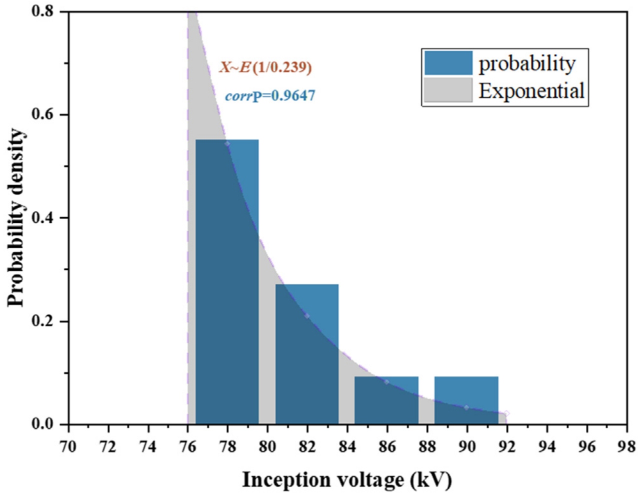

FIG. 3. Probability density of the laser-triggered positive streamer inception voltage.

voltage was selected to be 50% of the discharge voltage, ~1815 kV, as in the non-laser experiments. Thirty sets of discharge experiments were carried out, and the measured inception voltages were statistically analyzed (Fig. 6). Histograms showed that the negative streamer inception voltages with a laser filament applied ranged from −258 to 460 kV. Compared to the non-laser cases, the average value was close to −360 kV, almost unchanged, and the range decreased from 306.7 to 200.8 kV, which was less significant than that in the positive-polarity case. The effects of laser filaments on the streamer inception via a negative impulse were seen to be much less significant than those in the case of positive polarity.

B. Breakdown voltage and guidance results

The breakdown characteristics in a long air gap are influenced by the discharge initiation process and determined by the discharge development process. The breakdown discharge is often characterized by the 50% discharge voltage. The applied voltages here were all selected as 50% of the discharge voltages.

1. Effects of laser delay on discharge behavior

The guidance results for different laser delays in the form of marked points on the positive voltage waveform indicate three characteristic time periods of the laser incidence process (Fig. 7). t_{str} represents the moment of the first streamer inception, t_{lea} the moment of leader inception, and t_{in} the moment at which the laser was pumped into the discharge gap. Thus, $t_{in} < t_{str}$ is the time region before the first streamer inception, $t_{str} < t_{in} < t_{lea}$ is the dark period,[35] and $t_{in} > t_{lea}$ is the leader propagation period. Three effects were observed after the laser pumping. First, no discharge occurred at t_{in} and no guidance occurred after t_{in}. It mainly occurred during the leader propagation period, implying that, after the positive leader was initiated, the laser filament made almost no difference to the leader discharge. It also occupied the majority of the ex-streamer period. Second, discharge occurred at or around t_{in}, but no discharge developed along the filament, performing as a triggered discharge. When $t_{in} < t_{str}$, six triggered events were observed out of 30 experiments, and, when $t_{str} < t_{in} < t_{lea}$, 35 out of 60 triggered events were recorded, with the dark period becoming the time period with the highest probability of triggering positive discharges. Third, the discharge was not only initiated in advance by the laser filament but also propagated along the filament for certain lengths, resulting in a guided discharge. This type was, thus, included in the triggered events. Only four guided events were observed when $t_{in} < t_{str}$, and nine were observed when $t_{str} < t_{in} < t_{lea}$. Notably, the breakdown probability remained the same when $t_{in} < t_{str}$,

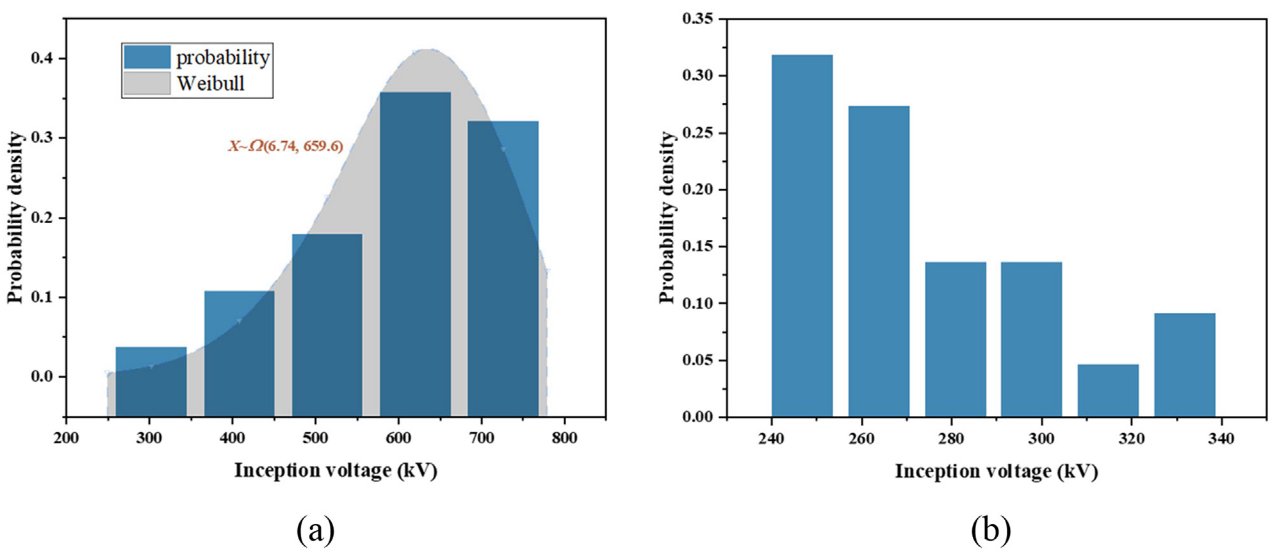

FIG. 4. Comparison of the positive leader inception voltage. (a) The probability density of the leader inception voltage and (b) the probability density of the laser-triggered leader inception voltage.

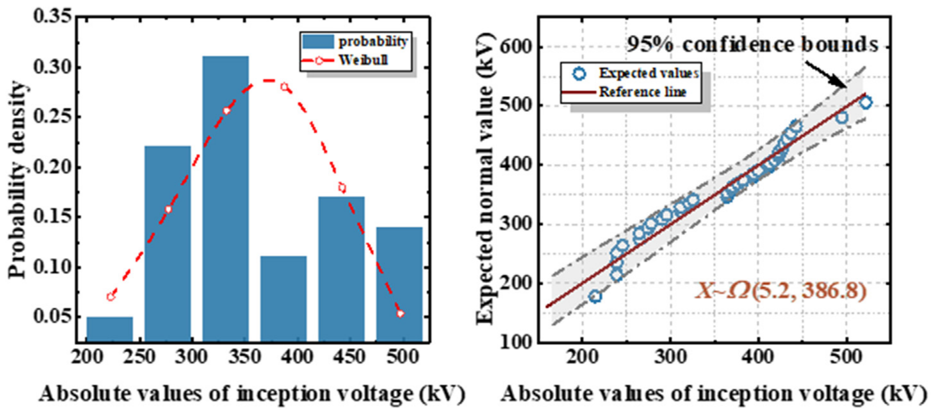

FIG. 5. Statistical analysis of the negative streamer inception voltage.

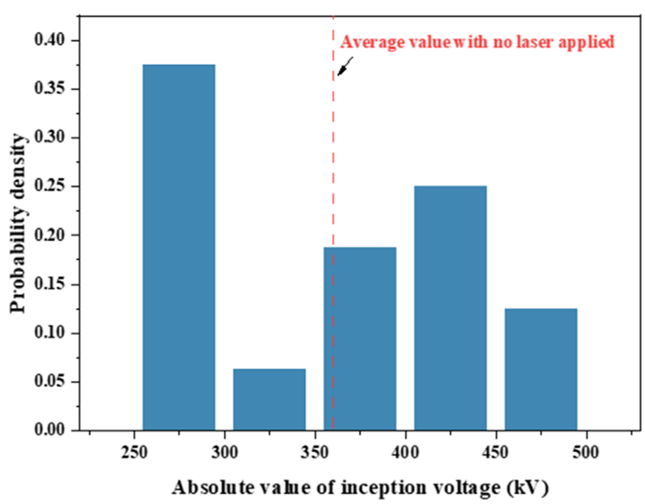

FIG. 6. Probability density of the laser-triggered negative streamer inception voltage.

and increased slightly from 50% to 56% when $t_{str} < t_{in} < t_{lea}$. For a positive discharge, the laser filament had a low probability of guiding the discharge passage but had little effect on the breakdown characteristics.

The guidance results for different laser delays in the form of marked points on the negative voltage waveform showed that the propagating duration of the negative leader was less than 5 ms, and the leader burst with extreme randomness (Fig. 8). Compared to the positive-polarity case, it was difficult to synchronize the laser delay with the negative leader propagation process. In this case, two characteristic time regions were identified for the laser incidence. When $t_{in} < t_{str}$, there was less impact on the discharge path and gap breakdown characteristics than in the positive-polarity case (Sec. III), but also little impact on the streamer inception. When $t_{in} > t_{str}$, a significant change in the discharge phenomenon was observed for t_{in} from 60 to 150 μs. All nine discharges were observed propagating along the laser path and all caused gap breakdown. The laser filament at this stage was observed to have a significant effect on the discharge path as well as the gap breakdown characteristics. To investigate the degree of laser filament contribution to the discharge at this stage,

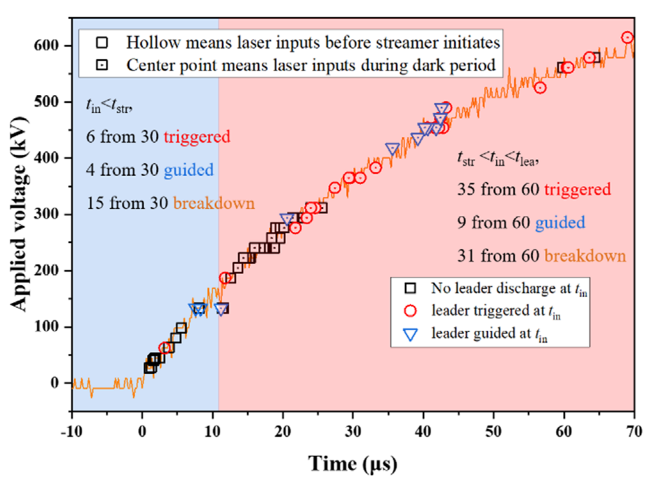

FIG. 7. Statistics of the positive discharge modes of the laser-engaged discharge.

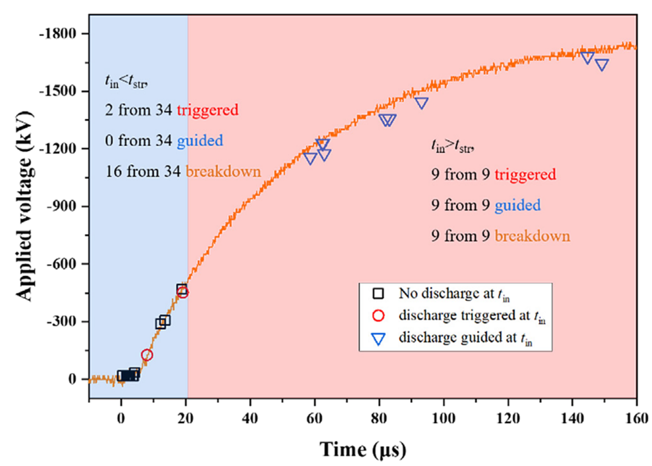

FIG. 8. Statistics of the negative discharge modes of the laser-influenced discharge.

further comparative experiments were performed by changing the laser delay and filament position.

IV. DISCHARGE BEHAVIORS

Based on the current and optical image observation system described in Sec. II, discharge processes and mechanisms were analyzed.

A. Positive discharge process

A typical positive discharge event was selected from a control group with no laser pumping [Fig. 9(a)]. When the applied voltage reached 201.1 kV (15.1 μs), a current pulse with an amplitude of 9.2 A was generated. The rise time was $\sim$30 ns, and the pulse duration stretched to $\sim$330 ns, representing the inception of the first streamer discharge. The discharge current then decayed to 0, representing suspended discharge activity entering the discharge stage of the dark period. The reason for this early streamer inception was that the radius of curvature at the end of the rod electrode was small enough to generate a strong electric field in the vicinity. However, the applied voltage at this moment was only 201.1 kV, which was too low to produce enough discharge energy to assist the transformation from a highly structured, dendritic streamer stem into a leader channel. At the same time, the migration speed of positive ions was too low to have a considerable displacement, forming a shield-like ion cover and obstructing recurring discharges. Therefore, after the first streamer process, the discharge activity in the gap was suspended. The dark period lasted about 55.8 μs. At $t = 71.5$ μs, the second current pulse was initiated with a rise time of tens of nanoseconds. The current reached 0.4 A and was sustained around that value for 38.1 μs, showing that the streamer stem had completed the transformation to the leader channel. Notably, the second current pulse turned into a continuous current, indicating that the leader propagated continuously and steadily in what is called a continuous stable leader discharge. At $t = 121.5$ μs, the

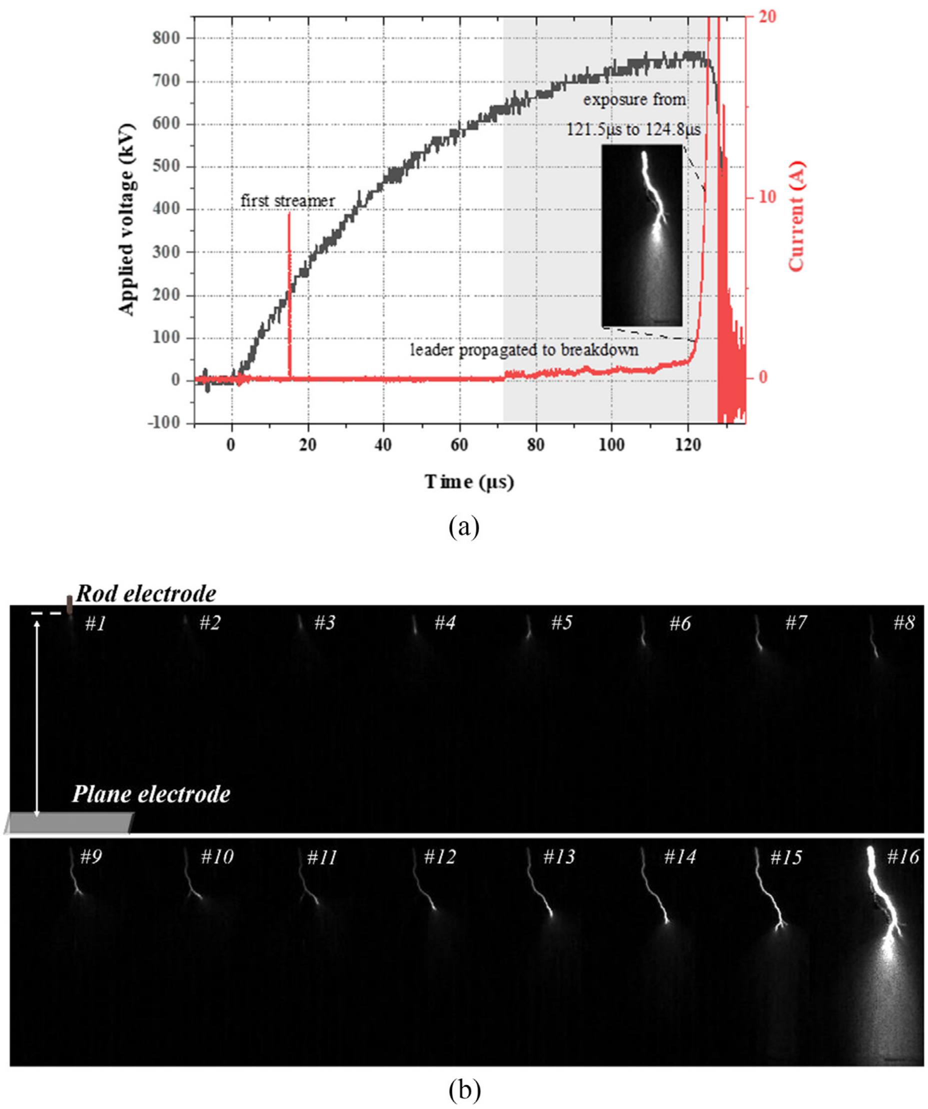

FIG. 9. Positive discharge behavior with no laser engaged. (a) Voltage and current pulses of typical discharge events and (b) enhanced processed high-speed video frames recording discharge before and after the emergence of separated luminous structures.

current increased steeply at a rate of 2.5 A/ns, representing the final jump through the discharge gap.

The evolution of the optical morphology characteristic of a typical discharge process was recorded [Fig. 9(b)]. The discharge morphology at the inception of a continuous stable leader is shown in frame #1, and frames #1 to #15 cover the continuous propagation process of the leader. The propagation speed was $\sim 1.5 \times 10^4$ m/s. In frame #16, the leader channel was connected to the plate electrode in the form of the final jump.

The voltage–current waveform of a typical laser-guided positive discharge showed that, as the applied voltage reached 197.5 kV (15.2 μs), the first streamer current pulse was generated [Fig. 10(a)] with an amplitude of 7.7 A. The rise time was $\sim$20 ns, and the pulse duration stretched to $\sim$280 ns, representing the natural inception of the first streamer discharge. At $t = 40.2$ μs, the laser was pumped during the dark period, leading to a current pulse with an amplitude of 1.4 A, which was 1 A (3.5 times) higher than that with no laser filament. Notably, the pulse peaked at $\sim$1 μs after t_{in} and was then transformed into a continuous current over 0.15 A, which was maintained for $\sim$15 μs until the final jump at $t = 77.2$ μs.

The optical morphology characteristic evolution of the guided discharge process was recorded [Fig. 10(b)]. The discharge morphology at the inception moment was recorded in frame #1, which is brighter than frame #1 in Fig. 9(b), but with no considerable differences in the discharge length. Frames #1 to #6 cover the continuous propagation of the leader discharge. The connection between the

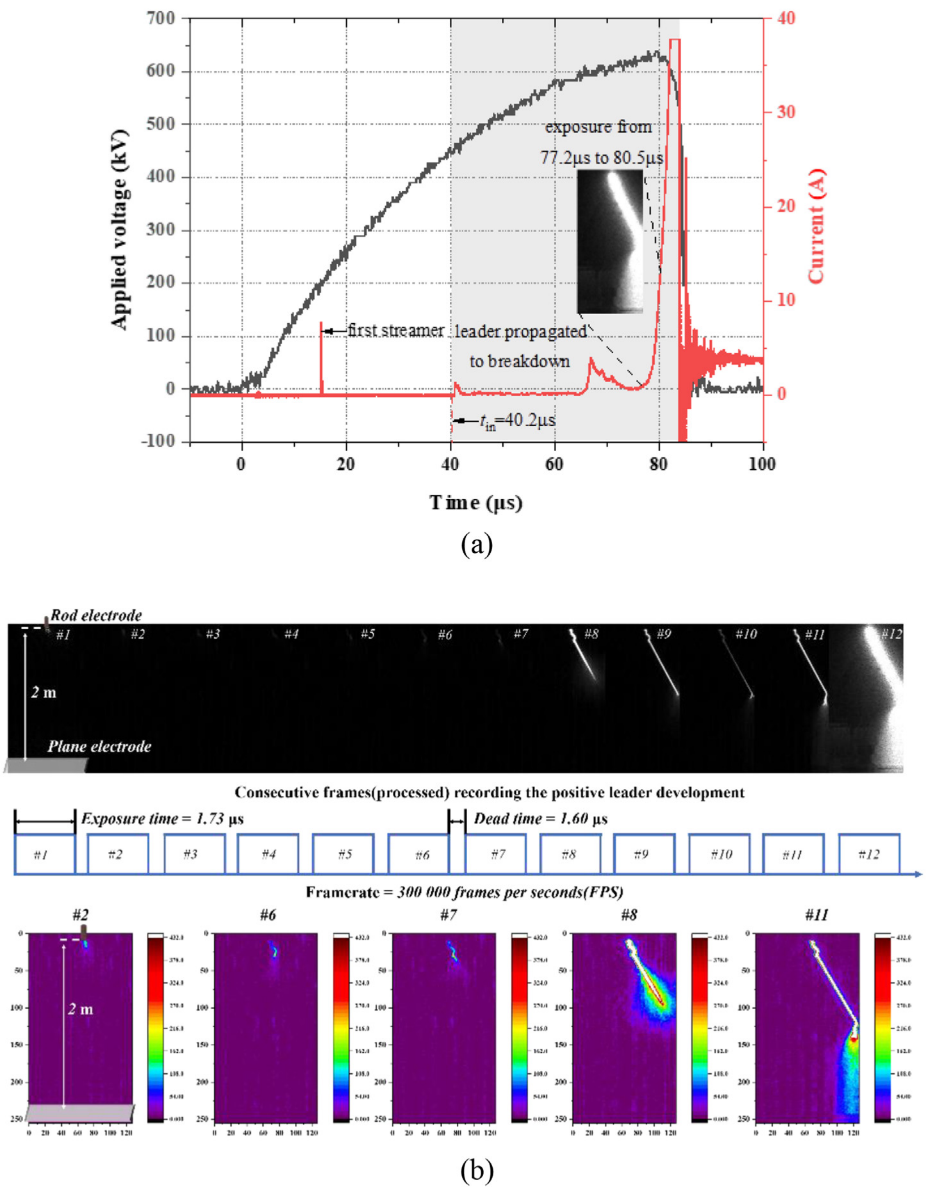

FIG. 10. Laser-guided positive discharge behavior. (a) Voltage and current pulses of a typical discharge event and (b) high-speed video frames. In the upper panel, enhanced processed high-speed video frames show the discharge before and after the emergence of separated luminous structures in gray images with a depth of 14 bits. The middle panel shows the exposure duration of each frame. In the bottom panel, pseudo-color images produced from the unprocessed gray frames are shown.

leader and laser filament channels was recorded in frame #7, corresponding to the current pulse at $t = 65$ μs. In frame #8, the leader channel propagated along the laser plasma channel with a speed of 10^5 m/s, corresponding to a current amplitude of 4 A and resulting in a strong streamer discharge at the end of the leader channel. The discharge then continued to propagate as the morphology of the leader connected to the rod electrode and a streamer at the head of the discharge channel.

B. Negative discharge process

Unlike positive discharge, negative discharge generally includes three discharge forms. The first is the negative leader, which is initiated from the rod electrode. The second is the space leader, which is initiated at a point in the gap and propagates to the rod electrode, possibly accompanied by reillumination after connecting with the negative leader. This reillumination phenomenon can prolong the original discharge channel. Finally, the positive leader is initiated from the rough or convex part of the plate electrode and propagates toward the rod electrode. The positive leader occurs during the final jump, which was not considered in this study. The ionized structure before the connection of the negative leader and the space leader was seen to be more complicated than that of the positive-polarity discharges. The negative discharge was distinguished from the positive mainly through the space leader. The space leader developed from an ionized zone as a "luminous nucleus" originating in the discharge gap, called the space stem, which was left independent in the gap by previous streamer discharges. This helped the negative discharge to propagate more than 2 m in air, rather than in the form of a continuous leader for positive discharge propagation. The streamers associated with the space stem propagated bidirectionally toward both electrodes. The positive streamer propagated and connected with the previous negative discharge, forming a spindle-shaped discharge area.

A typical voltage–current waveform of the space leader was selected from a control group with no laser pumping (Fig. 11). From the current waveform, the reillumination phenomenon was seen to correspond to a steep current front. The amplified current waveform and highspeed camera images showed that frames #1–3 recorded three consecutive frames of the bidirectional development of the streamers from the space leader (Fig. 11). Considering both the exposure and dead time of the camera, one frame took 1.11 μs in total. Before the connection of the space leader and negative leader channel, which corresponded to the steep front of the current waveform, stage A in the current waveform corresponded to a time of 2–3 frames recorded by

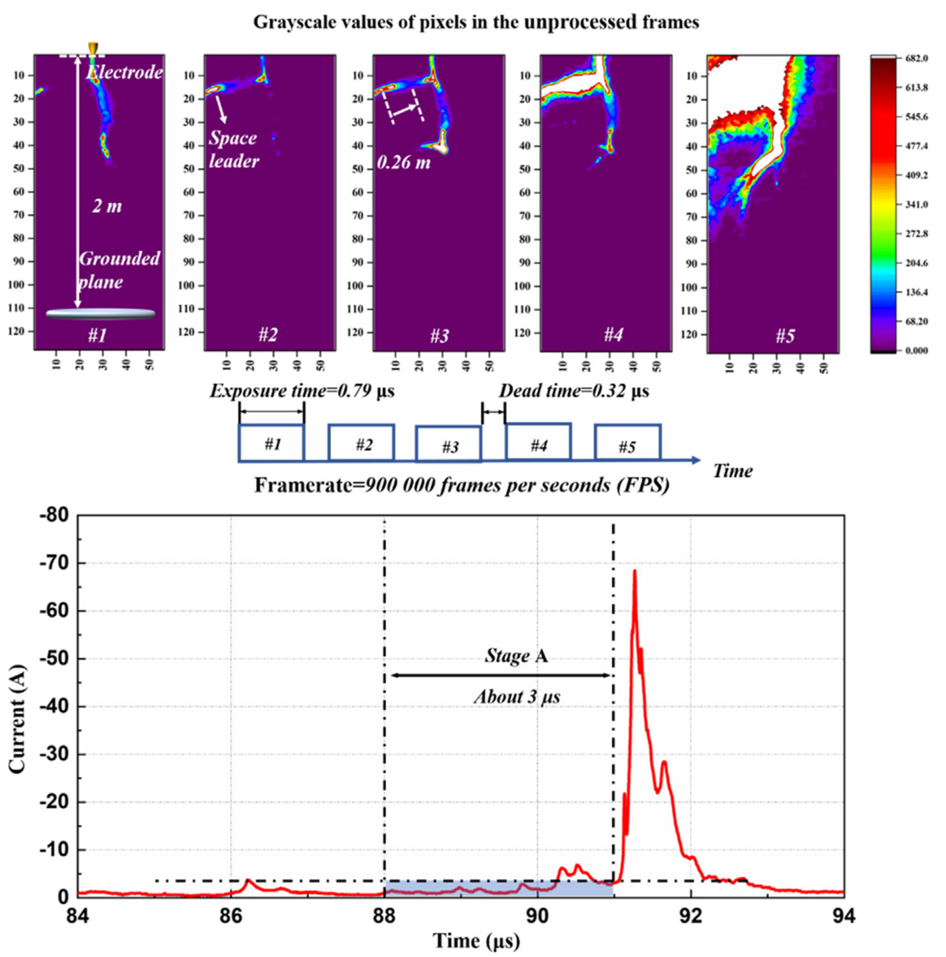

FIG. 11. Negative discharge behavior with no laser engaged. Voltage and current pulses of a typical discharge event. One major process of negative discharge development. In the upper panel, the pseudo-color images are transformed from unprocessed gray frames recorded at each step. These unprocessed frames are gray images with a depth of 14 bits. The dimensions of the grayscale matrix extracted from the unprocessed frames are 128 × 56. The colors of the pixels in the pseudo-color images represent values in the grayscale matrix. The deepest red corresponds to the maximum grayscale value of 682. The coordinate marked in the pseudo-color images represents the row and column numbers of the grayscale matrix. The middle panel shows the exposure duration of each frame, and the bottom panel shows an enlarged current pulse from 84 to 94 μs.

the camera, implicated the bi-directional propagation of the negative discharge and the discharge initiated from the space leader. The space leader lengthened during this phase of stable propagation with a higher velocity ($\sim$9 cm/μs) toward the cathode than that of the negative leader toward the space leader ($\sim$6 cm/μs). When the connection was completed, the current rose at a rate of $\sim$280 A/μs with the reillumination phenomenon.

For comparison purposes, the morphologies of the discharge and current waveforms were recorded. Although the connection part occurred too quickly to be recorded, similar current characteristics were observed. Before the steep current front, there was also a slowly increasing stage lasting $\sim$3 μs, corresponding to the connection phase between the space leader and negative leader channel. The connection point could be inferred from frame #3, and considering that the stage A interval was 0.03 μs, the propagation speed of the discharge initiated from the space leader was found to be $\sim$11 cm/μs toward the rod electrode, and the speed of the negative streamer was found to be $\sim$6 cm/μs toward the plate electrode, which was comparable with the no-laser case. A steep front then rose from 10% of the current peak (6.8 A) to 90% of the current peak (61.2 A) in 149 ns, optically observed as frames #1–2. The rising rate was $\sim$1.3 times greater than in the no-laser case, which cannot be regarded as a significant variation because of the dispersibility.

The voltage–current and charge quantity waveforms of a typical laser-guided negative discharge with the laser pumped at $t = 220$ μs were obtained [Fig. 12(a)]. Although the connection process between the filament and electrode could not be separately recorded by the camera, the process was determined from the current waveform. Comparing the current waveforms, the two discharge processes were found to have similar current characteristics, with both including a slow ramp-up stage and steep front stage before reaching peak values (Figs. 11 and 12). The closer streamer initiation point than the no-laser case resulted in a shorter duration of the increasing stage, and the plasma charge in the filament thus provoked a steeper front that rose from 10% of the current peak value to 90% in 24 ns. Statistical results showed that the current peak value was a multiple of 1–3 times that of the no-laser cases. The filament not only provided a steeper front but also a steeper falling edge, and the full pulse width reduced from 1 μs to $\sim$176 ns in this event. The discharge process with guidance from the filament was similar to the discharge process when connected to the space leader.

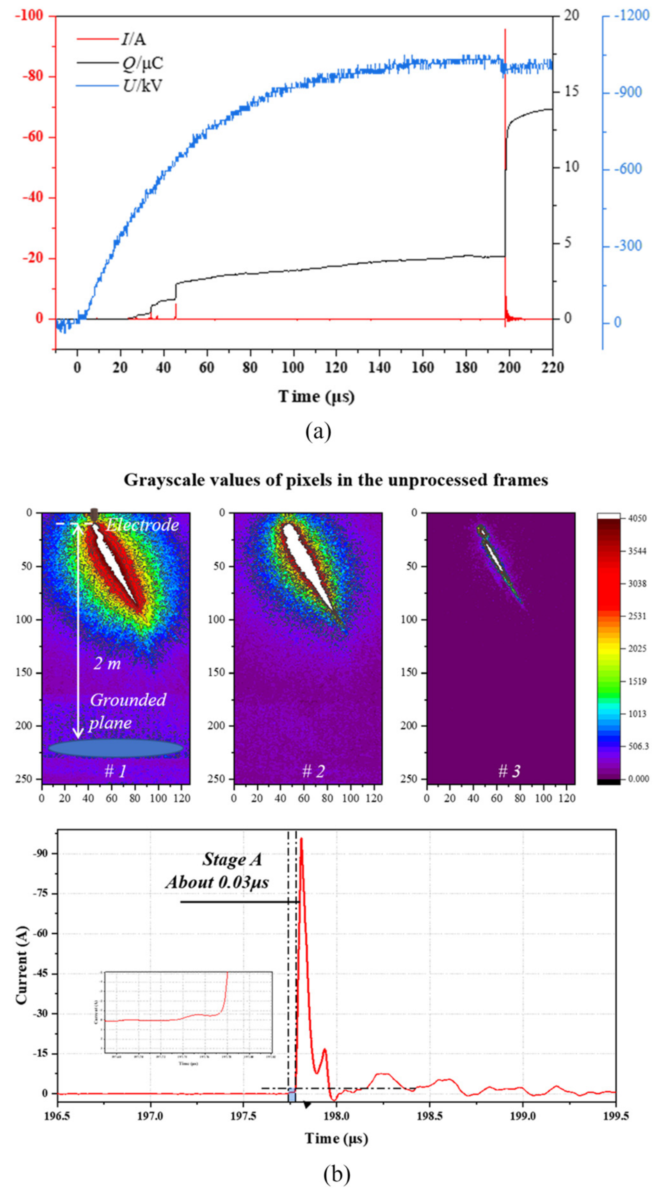

FIG. 12. Laser-guided negative discharge behavior. (a) Voltage and current pulses of a typical discharge event and (b) one major process of negative discharge development. In the upper panel, the pseudo-color images are transformed from unprocessed gray frame recordings at each step. These unprocessed frames are gray images with a 14 bit depth. The dimensions of the grayscale matrix extracted from the unprocessed frames were 256 $\times$ 128. The colors of the pixels in these pseudo-color images represent these values in the grayscale matrix. The deepest red corresponds to the maximum grayscale value of 4050. The coordinates marked in pseudo-color images represent row and column numbers of the grayscale matrix, and the bottom panel shows the enlarged current pulse from 196.5–199.5 μs.

V. DISCUSSIONS

The contributions of the laser filaments to the discharge process were analyzed based on two aspects: the contribution to the discharge inception and the contribution to the discharge propagation.

A. Differences between the effects of laser filaments on positive and negative discharge inceptions

Regarding discharge inception, studies by Comtois *et al.*[16] have made significant contributions to positive discharge inception. It was found that early laser input could not lead to advanced discharge inception. However, if the laser was pumped when the applied electric field was slightly stronger but still before the natural inception of the first streamer, advanced discharge inception was observed, in accordance with results in Sec. III, and valuable qualitative explanations for this were put forth. In this study, quantitative descriptions through a statistical analysis have been presented, based on time delay control and hundreds of experiments (30 of these were selected for the analysis). In addition, detailed studies on laser-influenced negative discharge inception have been lacking, but this was considered carefully in this study through the same experimental system and mathematical methods. This comparative study contributes to an understanding of laser effects on discharge inception characteristics with both polarities.

From Sec. III, for a positive discharge and an applied voltage at t_{in} less than the natural streamer inception voltage ($t_{in} = 0$–$10\ \mu s$), the laser filament was observed to change the positive streamer inception voltage distribution from a Weibull to an exponential distribution. However, this also reduced the average value of the inception voltage by 65.2% and the range by 88.5%. For a negative discharge, laser filaments had little impact on the breakdown voltage or the average value of the inception voltage, with the inception voltage range only decreasing by 34.4%. The huge differences between the two polarities were analyzed. At the moment the laser entered the gap, the air was weakly ionized by multi-photon absorption, where the electron density was determined by the peak power and area of the laser beam. The migration and accumulation of photoelectrons were ongoing under the applied electric field, distorting the local electric field, especially at the ends of the laser filament. As the supply of seed electrons and the local electric field increased, an electron avalanche occurred, and it was easier to achieve an avalanche-to-streamer transition. However, for different polarities of the applied electric field, the migration and accumulation of particles were different, resulting in a different impact on the avalanche-to-streamer transition. Therefore, the contribution of laser filaments to discharge inception mainly depended on three processes—photoelectron generation, migration, and accumulation—as well as the distortion of the local electric field by the post-filament.

For positive polarity, ionized electrons in the air moved toward the rod electrode. As the laser beam was 1 cm away from the rod end surface, at a migration speed of 0.2×10^6 m/s, only a nanosecond-length delay was needed for electrons entering the strong electric field area. This migration caused local distortion of the electric field and, thus, ionization as well as the avalanche. For negative polarity, electrons appearing in the gap moved away from the strong electric field area toward the ground electrode at a decreasing speed. Although the heavier positive ions of the filament plasma moved toward the rod, the speed was too slow for a certain distance to distort the field, with a group of positive space charges left 1 cm from the rod electrode. In this case, it was only when electrons formed on the rod surface and entered the strong electric field area that the electron avalanche occurred. When the avalanche developed to the positive space-charge area, the probability of forming a self-sustaining discharge increased. The quantitative estimates of the electric field distortion will be discussed in more detail in the simulation part in Discussion B.

The discharge stage in sync with the laser filaments played a decisive role in the laser contribution to different polarity discharges. When the laser was pumped in the gap after the natural streamer inception, the effect was reversed. Although the applied voltage had reached the voltage for discharge inception, the electric field in front of the rod was weakened by the preceding streamer process. However, if the electric field distribution interfered with the re-satisfaction of the discharge inception, the discharge could be initiated in advance during the dark period. From the experimental results in Sec. IV, after the laser was seen to enter the discharge gap, regardless of positive or negative polarity, the discharge could be initiated, only with different probabilities, indicating that the laser filament plasma had a significant effect on the electric field distribution. As long as the weakening from the space charges was supplemented, the superimposed electric field, formed by the applied voltage and space charge, increased to satisfy the discharge inception condition again, such that recurring discharge could be reinitiated.

During the discharge propagation stage, the discharge channel was transformed from the streamer to the leader channel (internal temperature of the channel > 1500 K[36]) The enhancement effect of the laser filament plasma on the local electric field was far less than that of the leader channel directly connected to the rod electrode, such that a new streamer discharge could not be re-initiated during this period.

B. Differences between the effects of laser filaments on positive and negative discharge propagations

In previous studies,[16] laser-guided positive discharge events were only occasionally observed during the dark period, which is consistent with the finding in this work that the possibility of laser filaments triggering a guided leader is the biggest with t_{in} during the dark period but does not occur with t_{in} during the leader propagation.

In Sec. III, it was seen that the contribution of laser filaments to positive discharge propagation mainly converged on the dark period. Nevertheless, the effects of nine guidance events from 60 events indicated a lower probability of 15% compared with the laser-guided negative-polarity discharge. The low guidance probability indicated that the breakdown probability was not significantly increased. In addition, it was found in this study that when $t_{in} < t_{str}$, there was also a small possibility of guiding a leader discharge. This phenomenon was related to thermodynamic processes, which heated up the filament more than 100 K,[37] turning the filament into a thin hot wire. With gas expansion, the gas number density N in the filament decreased and, thus, the area with reduced electric field E/N was more likely to guide the discharge propagation. For $t_{in} < t_{str}$, the time interval between t_{in} and t_{lea} was dozens of μs, which was much larger than the dissipation time of the plasma. However, the heating channel could be maintained for several ms, which allowed the leader discharge to propagate along the left heating channel. Without the attraction by a distorted electric field produced by plasmas, the guiding possibility appeared much less than t_{in} during the dark period.

For negative discharges, the space stem formed by laser filaments was observed in previous studies,[17] revealing that laser-guided negative discharges may obey similar mechanisms to natural negative discharges. In this study, low-noise current waveforms were recorded from which two discharge periods were confirmed. Furthermore, by comparative study, the current waveform characteristics provided more evidence of the underlying mechanism, in which the laser filament acted as a space stem in the discharge propagation stage. It was also shown that the laser-guided positive and negative discharges had different mechanisms.

The experiments from Sec. III showed that the guidance probability exceeded 95%; that is, as long as the applied voltage reached the streamer inception voltage, laser filaments could offer a rather high probability of guiding the discharge path to propagate along the laser compared to the positive-discharge case. From Sec. IV, it seemed that the discharge guidance probability depended on the connection process of the discharge initiated from the rod electrode and discharge initiated from the laser plasma, corresponding to the slow-rising phase in the current waveform. The slow ramp-up time of the current waveform was seen to be produced by a laser-guided negative-polarity discharge of 0.03 μs before the steep wavefront, while in the positive

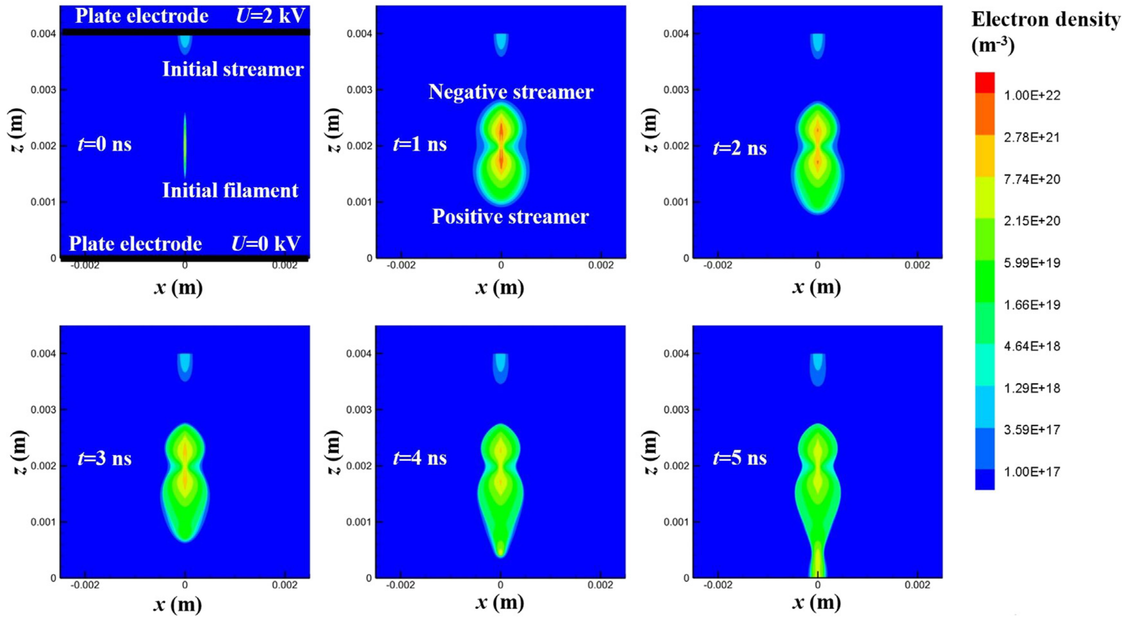

FIG. 13. Evolution of the electron density distribution of the filament under a uniform background electric field.

discharge case, the current peaked at $\sim 1\ \mu s$ only with a steep wavefront (Figs. 10 and 12). Such differences in the current waveforms of the connection process were related to the connection modes of the rod discharge and laser filaments, and a possible conjecture was put forth here. The condition for the positive discharge propagating along laser filaments involved the positive leader being initiated from the rod electrode, which coincided with the laser plasma channel in the spatial position during the propagation process. The condition for the negative discharge propagating along laser filaments involved the connection of bi-directional discharges, which were the negative leader discharge from the rod electrode and the positive streamer from the laser filament.

To further examine this conjecture, a simulation model was constructed. A uniform background electric field of 5 kV/cm was represented by a 4 mm plate-plate gap with DC voltage and a 1 mm filament plasma placed in the middle position of the gap. The governing equations can be found in Ref. 38. The discharge process of the filament plasma under the background electric field with an anodic upper plate is shown in Fig. 13. The discharges from the filament plasma were seen to develop on both sides in the form of bipolar streamers. The positive streamer developed until it connected with the cathode, while the negative streamer could not meet the conditions for streamer discharge due to the outward electron diffusion. Under experimental conditions, a similar inference was drawn. During the positive leader propagation phase, the negative streamer at the end of the laser plasma could not effectively develop to form an electric field distribution that could attract the positive leader. Thus, it was only when the positive leader developed to the filament plasma channel that guidance could form with a low probability. During the negative leader propagation phase, the positive streamer at the end of the laser plasma could develop toward the rod under the integrative electric field. The bi-directional development of discharges greatly improved the probability of connection between the two channels.

The evolution of the axial electric field is shown in Fig. 14, where the plate connected to the ground is at $z = 0$ and 2 kV is at $z = 0.004$ m. Electric field distortions were seen to occur at both ends of the filament with different directions, formed by charge accumulation after polarization. The electric field approaching the cathode was in the direction of the applied field, while the field approaching the anode was in the opposite direction. At $t = 1$ ns, the distorted electric field in front of the positive streamer reached ~ 90 kV/cm and developed at a speed of $\sim 18\ \text{cm}/\mu s$, which was similar to that of the observed

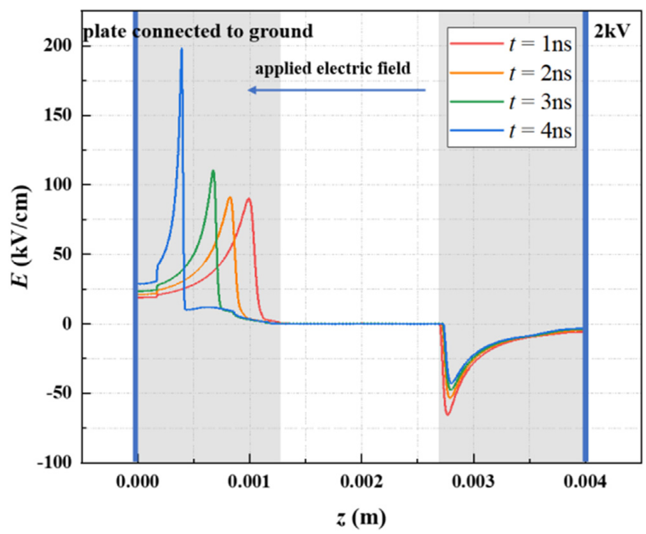

FIG. 14. Evolution of the electric field distribution of a filament under a uniform background electric field.

discharge in a long-air-gap experiment with a negative voltage applied. The field approaching the anode was also seen to be distorted but did not transform into a discharge propagation due to the field shielding from negative ions combined with electrons migrating to the anode and neutral particles. As the positive ions were relatively static at the other end of the filament, the propagation of negative discharges was much more difficult than that of positive discharges. Correspondingly, in long-air-gap experiments with a positive voltage applied, ionization activities at the end of the filament were not able to affect the electric field in front of the electrode but only able to provide seed electrons, such that the contribution to negative discharges was seen to be less than that of positive discharges.

Although this simulation tool can offer valuable insight into specific aspects of the gas discharge phenomenon, it cannot yet account for the dynamic processes relevant to leader or breakdown discharges in long air gaps. The present work is thus meant to focus on the dynamical processes relevant to plasma evolution from laser filaments under an applied electric field, and provides a valuable reference for the analysis of the contribution of laser filaments to discharges of both polarities.

VI. CONCLUSIONS

In this study, rod-to-plate air gap discharge experiments under switching impulses of both positive and negative polarities were carried out. Based on a synchronous system of laser, impulse, and measurement devices, the discharge processes were characterized by current waveforms and optical images. The inception, propagation, and breakdown characteristics of discharges of both polarities were analyzed statistically. The differences between the laser filament contributions to each polarity discharge were discussed. The guidance mechanism was further investigated through a simulation model. The main conclusions were as follows:

(a) Statistical results under a 50% discharge voltage of 821 kV showed that positive natural streamer and leader inception voltages were strongly dispersive and obeyed a Weibull distribution. When the laser was pumped at $t_{in} < t_{str}$, the streamer and leader inception voltage were both strongly dropped over 50%, also with a reduced dispersion. The probability distributions were transformed into an exponential distribution.

(b) The contribution of laser filaments to negative-polarity discharge inception was significantly less than their contribution to positive-polarity inception. With the laser pumped at $t_{in} < t_{str}$, the inception voltage characteristics, including the mean value, dispersion, and probability distribution, had little changes from natural negative discharge cases.

(c) The contribution of laser filaments to discharge inception was speculated to include three processes: (1) Air is weakly ionized by multiphoton absorption or tunneling ionization, generating ionized particles in front of the electrode. (2) Photoelectrons migrate and accumulate under the applied electric field, thus affecting the local electric field. (3) As the local supply of seed electrons and the electron growth environment (electric field distribution) are changed, the streamer is generated with different characteristics under the same mechanism. Under the applied voltages of different polarities, the different migration directions of photoelectrons lead to differences in laser effects on the inception of positive- and negative-polarity discharges.

(d) Statistical results showed that the guidance probability of positive discharge could reach 15% when the laser was pumped during the dark period stage, leading to little effect on the breakdown discharge probability.

(e) Statistical results showed that the guidance probability of the negative discharge could exceed 95% during the dark period. Under the applied voltages of different polarities, the different connection probabilities led to differences in laser effects on the propagation of positive- and negative-polarity discharges.

(f) The difference in the connection of a discharge initiated from the rod electrode with the laser plasma channel was speculated to lead to differences in the guidance probability. The connection condition for a positive discharge was that the positive leader propagated until it was superimposed on the laser plasma channel. The connection condition for negative discharge was that the discharge initiated from the rod electrode connected to the positive streamer initiated from the end of the laser plasma channel through bi-directional discharge propagation.

SUPPLEMENTARY MATERIAL

See the supplementary material for the details of the simulation of laser plasma dynamics under a uniform electric field.

ACKNOWLEDGMENTS

This work was financially supported by the Science and Technology Project of SGCC (Research on Femtosecond Laser Triggered Discharge in Long Air Gap, Project No.: 52120519003H).

AUTHOR DECLARATIONS

Conflict of Interest

The authors have no conflicts to disclose.

Author Contributions

Zhehao Pei: Conceptualization (lead); Data curation (equal); Formal analysis (equal); Investigation (lead); Methodology (lead); Resources (equal); Software (lead); Writing – original draft (lead); Writing – review & editing (lead). **Rui Zhang:** Methodology (equal). **Qiao gen Zhang:** Funding acquisition (supporting); Methodology (supporting); Project administration (equal); Resources (equal); Supervision (equal); Writing – review & editing (supporting). **Weijiang Chen:** Conceptualization (equal); Funding acquisition (lead); Methodology (equal); Project administration (lead); Resources (lead); Supervision (lead); Writing – review & editing (equal). **Xing Fan:** Formal analysis (lead); Investigation (equal); Writing – review & editing (supporting). **Jianwei Gu:** Investigation (equal); Resources (equal). **Shengxin Huang:** Formal analysis (equal); Project administration (equal); Supervision (equal); Validation (equal); Writing – review & editing (equal). **Xiaosong Liu:** Data curation (equal). **Zhong Fu:** Project administration (equal); Resources (equal). **Bin Du:** Project administration (equal). **Tie-Jun Wang:** Formal analysis (supporting); Writing – review & editing (supporting).

DATA AVAILABILITY

The data that support the findings of this study are available from the corresponding author upon reasonable request.

REFERENCES

[1]E. M. Bazelyan and Y. P. Razier, *Lightning Physics and Lightning Protection* (IOP, Bristol, UK, 2000).
[2]C. Tong, in 30th International Conference on Lightning Protection, Cagliari, Italy (2010).
[3]N. Khan, N. Marium, I. Aris, and J. Yeak, New J. Phys. **4**, 61 (2002).
[4]L. Cai, J. Li, J. Wang, R. Su, Y. Ke, M. Zhou, and Q. Li, Geophys. Res. Lett. **48**(11), e2021GL093483, https://doi.org/10.1029/2021GL093483 (2021).
[5]D. W. Koopman and K. A. Saum, J. Appl. Phys. **44**(12), 5328 (1973).
[6]A. Braun, G. Korn, X. Liu, D. Du, J. Squier, and G. Mourou, Opt. Lett. **20**(1), 73 (1995).
[7]S. L. Chin, *Femtosecond Laser Filamentation* (Springer Science + Business Media, LLC, New York, 2010), Vol. 55.
[8]S. L. Chin, A. Brodeur, S. Petit, O. G. Kosareva, and V. P. Kandidov, J. Nonlinear Opt. Phys. Mater. **8**(1), 121 (2012).
[9]S. Tzortzakis, L. Berge, A. Couairon, M. Franco, B. Prade, and A. Mysyrowicz, Phys. Rev. Lett. **86**(24), 5470 (2001).
[10]S. Tzortzakis, M. A. Franco, Y. B. Andre, A. Chiron, B. Lamouroux, B. S. Prade, and A. Mysyrowicz, Phys. Rev. E **60**(4), 3505 (1999).
[11]A. Couairon and A. Mysyrowicz, Phys. Rep. **441**(2–4), 47 (2007).
[12]R. P. Fischer, A. C. Ting, D. F. Gordon, R. F. Fernsler, G. P. DiComo, and P. Sprangle, IEEE Trans. Plasma Sci. **35**(5), 1430 (2007).
[13]A. Malagon-Romero and A. Luque, Geophys. Res. Lett. **46**(7), 4029, https://doi.org/10.1029/2019GL082063 (2019).
[14]S. X. Huang, W. J. Chen, Z. H. Pei, Z. Fu, L. F. Wang, T. Y. He, Z. J. Li, J. W. Gu, K. Bian, N. W. Xiang, and Y. Wang, Geophys. Res. Lett. **47**(3), e2019GL086183, https://doi.org/10.1029/2019GL086183 (2020).
[15]J. Gu, S. Huang, Y. Fu, W. Chen, D. Cheng, W. Shi, Z. Fu, Z. Pei, X. Fan, and T. He, J. Phys. D **54**(2), 025205 (2021).
[16]D. Comtois, H. Pepin, F. Vidal, F. A. M. Rizk, C. Ching-Yuan, T. W. Johnston, J. Kieffer, B. La Fontaine, F. Martin, C. Potvin, P. Couture, H. P. Mercure, A. Bondiou-Clergerie, P. Lalande, and I. Gallimberti, IEEE Trans. Plasma Sci. **31**(3), 377 (2003).
[17]R. Ackermann, G. Méchain, G. Méjean, R. Bourayou, M. Rodriguez, K. Stelmaszczyk, J. Kasparian, J. Yu, E. Salmon, S. Tzortzakis, Y. B. André, J. F. Bourrillon, L. Tamin, J. P. Cascelli, C. Campo, C. Davoise, A. Mysyrowicz, R. Sauerbrey, L. Wöste, and J. P. Wolf, Appl. Phys. B **82**(4), 561 (2005).
[18]B. Forestier, A. Houard, I. Revel, M. Durand, Y. B. André, B. Prade, A. Jarnac, J. Carbonnel, M. Le Nevé, J. C. de Miscault, B. Esmiller, D. Chapuis, and A. Mysyrowicz, AIP Adv. **2**(1), 012151 (2012).
[19]A. Houard, P. Walch, T. Produit, V. Moreno, B. Mahieu, A. Sunjerga, C. Herkommer, A. Mostajabi, U. Andral, Y.-B. André, M. Lozano, L. Bizet, M. C. Schroeder, G. Schimmel, M. Moret, M. Stanley, W. A. Rison, O. Maurice, B. Esmiller, K. Michel, W. Haas, T. Metzger, M. Rubinstein, F. Rachidi, V. Cooray, A. Mysyrowicz, J. Kasparian, and J.-P. Wolf, arXiv:2207.03769 (2022).
[20]A. Desparois, B. L. Fontaine, A. Bondiou-Clergerie, C. Chien, D. Comtois, T. W. Johnston, J.-C. Kieffer, H. P. Mercure, H. Pepin, F. A. M. Rizk, and F. Vidal, IEEE Trans. Plasma Sci. **28**(5), 1755 (2000).
[21]B. L. Fontaine, D. Comtois, C.-Y. Chien, A. Desparois, F. Genin, G. Jarry, T. Johnston, J.-C. Kieffer, F. Martin, R. Mawassi, H. Pepin, F. A. M. Rizk, and F. Vidal, J. Appl. Phys. **88**(2), 610 (2000).
[22]M. Rodriguez, R. Sauerbrey, H. Wille, L. Woste, T. Fujii, Y. B. Andre, A. Mysyrowicz, L. Klingbeil, K. Rethmeier, W. Kalkner, J. Kasparian, E. Salmon, J. Yu, and J. P. Wolf, Opt. Lett. **27**(9), 772 (2002).
[23]S. Eto, A. Zhidkov, Y. Oishi, M. Miki, and T. Fujii, Opt. Lett. **37**(6), 1130 (2012).
[24]L. Arantchouk, G. Point, Y. Brelet, B. Prade, J. Carbonnel, Y. B. André, A. Mysyrowicz, and A. Houard, J. Appl. Phys. **116**(1), 013303 (2014).
[25]S. Nijdam, E. Takahashi, J. Teunissen, and U. Ebert, New J. Phys. **16**, 103038 (2014).
[26]T. Fujii, K. Sugiyama, A. Zhidkov, M. Miki, E. Hotta, and K. Nemoto, in *Progress in Ultrafast Intense Laser Science XI* (Springer, 2015), p. 195.
[27]A. Schmitt-Sody, D. French, W. White, A. Lucero, W. P. Roach, and V. Hasson, Appl. Phys. Lett. **106**(12), 124101 (2015).
[28]K. Cvecek, B. Gröschel, and M. Schmidt, Phys. Proc. **83**, 587 (2016).
[29]F. Theberge, J. F. Daigle, J. C. Kieffer, F. Vidal, and M. Chateauneuf, Sci. Rep. **7**, 40063 (2017).
[30]E. W. Rosenthal, I. Larkin, A. Goffin, T. Produit, M. C. Schroeder, J. P. Wolf, and H. M. Milchberg, Opt Express **28**(17), 24599 (2020).
[31]T.-J. Wang, J. Zhang, Z. Zhu, Y. Liu, N. Chen, H. Guo, H. Sun, Y. Leng, S. Leang Chin, and R. Li, AIP Adv. **10**(3), 035128 (2020).
[32]G. Point, "Energy deposition from femtosecond laser filamentation for the control of high voltage spark discharge," Ph.D. thesis (Ecole Polytechnique, 2015).
[33]S. Mitryukovskiy, Y. Liu, P. Ding, A. Houard, A. Couairon, and A. Mysyrowicz, Phys. Rev. Lett. **114**(6), 063003 (2015).
[34]R. Zhang, Q. Zhang, J. Zhou, C. Guo, X. He, Z. Wu, and T. Wen, J. Phys. D **55**(6), 065501 (2021).
[35]Y. Razier, *Gas Discharge Physics* (Springer-Verlag, Berlin, 1991).
[36]I. Gallimberti, J. Phys. Colloq. **40**(C7), 193–250 (1979).
[37]S. Tzortzakis, B. Prade, M. Franco, A. Mysyrowicz, S. Huller, and P. Mora, Phys. Rev E **64**(5), 057401 (2001).
[38]X. Chen, Y. Zhu, and Y. Wu, Plasma Sources Sci. Technol. **29**(9), 095006 (2020).